BLADE FRAGMENT OF A WINGED AXE FK43 – TIN BRONZE – MIDDLE BRONZE AGE – SWITZERLAND

Artefact name	Blade fragment of a winged axe FK43
Authors	Marianne. Senn (EMPA, Dübendorf, Zurich, Switzerland) & Christian. Degrigny (HE-Arc CR, Neuchâtel, Neuchâtel, Switzerland)
Url	/artefacts/343/

The object

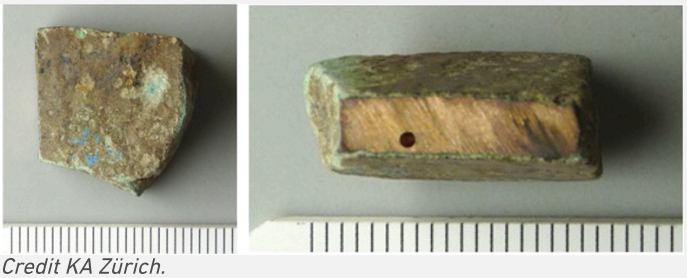

Credit KA Zürich.

Fig. 1: Tin bronze tool fragment. The drilling on the right picture was carried out at a later stage and does not form part of the original object,

Description and visual observation

Description of the artefact	Blade fragment of a semi-finished median-winged axe. Its surface is covered with a thick dark green corrosion crust (Fig. 1). Dimensions: L = 20mm; Tmax. = 8.5mm; WT = 15g.
Type of artefact	Tool
Origin	Obstgartenstrasse, Erlenbach, Zurich, Switzerland
Recovering date	Excavation 1980.002
Chronology category	Middle Bronze Age
chronology tpq	1550 B.C.
chronology taq	1350 B.C.
Chronology comment	1550BC _ 1350BC
Burial conditions / environment	Soil
Artefact location	Kantonsarchäologie, Dübendorf, Zurich
Owner	Kantonsarchäologie, Dübendorf, Zurich
Inv. number	FK43
Recorded conservation data	Not conserved

This work is licensed under CC BY-NC-ND 4.0

Complementary information

Nothing to report.

Study area(s)

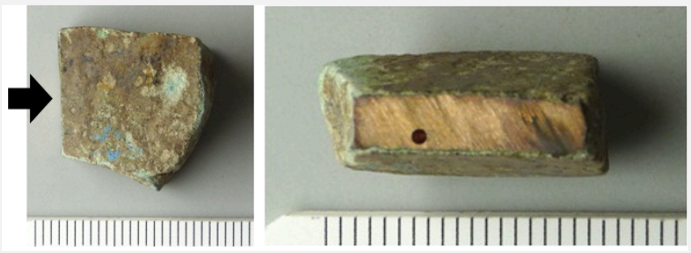

Credit HE-Arc CR.

Fig. 2: Location of sampling area (arrow, left picture) and side view (right picture),

Binocular observation and representation of the corrosion structure

Stratigraphic representation: none.

MiCorr stratigraphy(ies) – Bi

Sample(s)

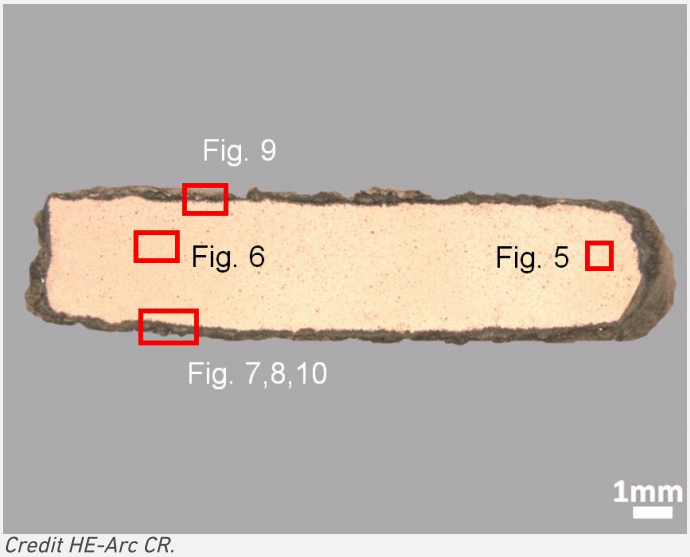

Credit HE-Arc CR.

Fig. 3: Micrograph of the cross-section showing the location of Figs. 5 to 10,

Description of sample	The sample was cut from the fragment shown in Fig. 2. The cross-section is rectangular in shape (L = 17mm, W= 4mm) and has a thick corrosion crust (Figs. 2 and 3).
Alloy	Tin Bronze
Technology	As-cast

This work is licensed under CC BY-NC-ND 4.0

Lab number of sample	ERL-43
Sample location	Begbroke Science Park (Peter Northover), Yarnton, England
Responsible institution	Kantonsarchäologie, Dübendorf, Zurich
Date and aim of sampling	Date unknown, metallography and chemical analyses

Complementary information

Nothing to report.

Analyses and results

Analyses performed:
Metallography (etched with ferric chloride reagent), Vickers hardness testing, SEM/EDS, EPMA/WDS, Raman spectroscopy.

Non invasive analysis

Metal

The remaining metal is a tin bronze (Table 1) with high porosity and grey copper sulphide inclusions (Figs. 5 and 6, Table 2). The etched metal has the typical dendritic structure of a cast tin bronze with an average hardness of HV1 135 (Fig. 6). The cored dendritic structure is surrounded by an alpha-delta eutectoid. The core of the dendrites is rich in Cu whereas the outer layers are rich in Sn.

Elements	Cu	Sn	As	Fe	Ni	Pb	Sb	Co	Ag	Au	Zn	Bi	Si
mass%	85.14	11.95	1.54	0.49	0.39	0.18	0.14	0.13	0.02	0.02	<	<	n. d.

Table 1: Chemical composition of the metal. Method of analysis: EPMA/WDS, Lab Department of Materials, University of Oxford.

Elements	Cu	S	Fe	Total
Dark-grey inclusion	66	24	10	100

Table 2: Chemical composition (mass %) of the dark-grey inclusions seen in Fig. 5. Method of analysis: SEM/EDS, Laboratory of Analytical Chemistry, Empa.

This work is licensed under CC BY-NC-ND 4.0

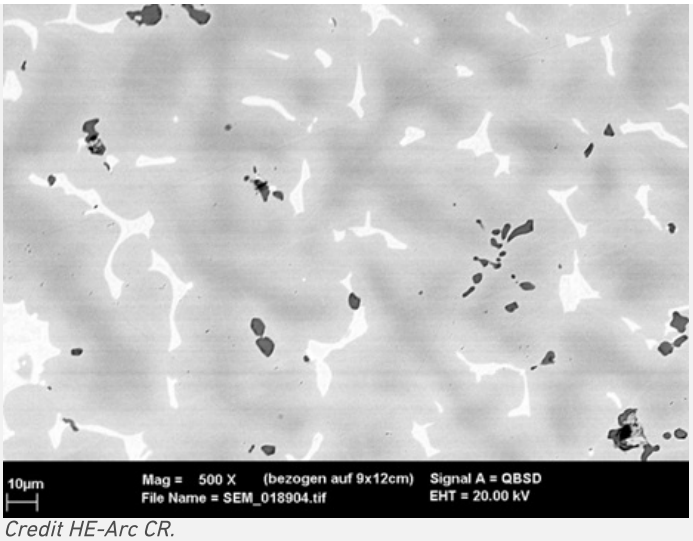

Credit HE-Arc CR.

Fig. 5: SEM image of the metal sample from Fig. 3 (detail), BSE-mode. The cored alpha phase of the dendrites appears in grey, becoming lighter towards the periphery (more Sn). The alpha-delta eutectoid appears in white and the copper sulphide inclusions in dark-grey,

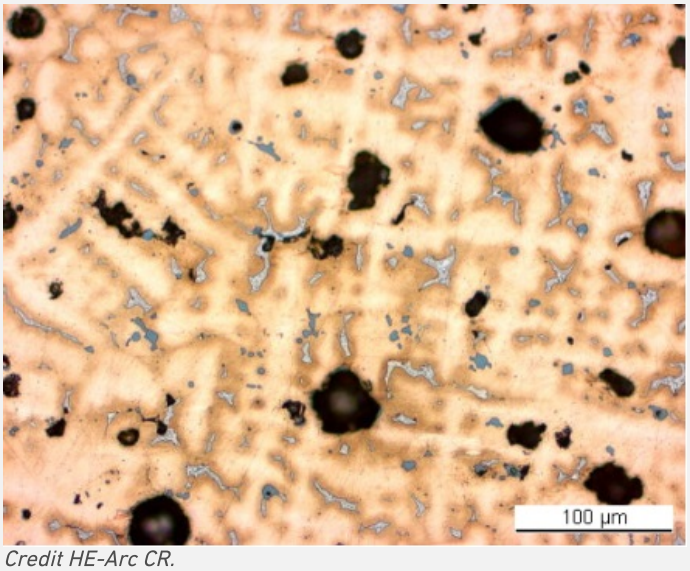

Credit HE-Arc CR.

Fig. 6: Micrograph of the metal sample from Fig. 3, etched, bright field. We observe the eutectoid phase in light grey and copper sulphide inclusions in dark-grey,

Microstructure	Dendritic structure + strain lines (metal surface)
First metal element	Cu
Other metal elements	As, Sn

Complementary information

Nothing to report.

Corrosion layers

A dark green corrosion crust with a thickness between 100 and 320µm covers the entire surface of the blade fragment (Fig. 7). It retains a metallic ghost structure (Sn-rich eutectoid alpha + delta phase). Under polarized light localized orange and red corrosion products can be seen at the metal - corrosion crust interface (Fig. 8). Interdendritic corrosion and corroded slip lines can be seen in the metal structure and near fissures (Fig. 9). Elemental mapping (Fig. 10) shows that the green layer is Sn-rich (CP1, probably cassiterite, SnO_2) and depleted of Cu, whereas the orange and red corrosion particles are depleted of Sn and rich in Cu (Fig. 10, Table 3). Their Raman spectra indicate that they are mainly composed of cuprite (Fig. 11). The overall corrosion crust contains O, Si, C and Fe from the environment, while S is concentrated around the cuprite particles (Fig. 10).

Elements	O	Si	P	Fe	Ni	Cu	As	Sn	Total
Surface CP1	43	0.8	<	6.2	<	16	1	43	111

This work is licensed under CC BY-NC-ND 4.0

Middle CP1	42	1.7	0.7	12	<	10	0.7	43	110
Red/orange CP in CP1	41	0.9	<	4.4	<	36	<	22	104
Remnant metal phase	9	0.7	<	5	0.8	34	<	47	97

Table 3: Chemical composition (mass %) of the corrosion crust from Fig. 7. Method of analysis: SEM/EDS, Laboratory of Analytical Chemistry, Empa.

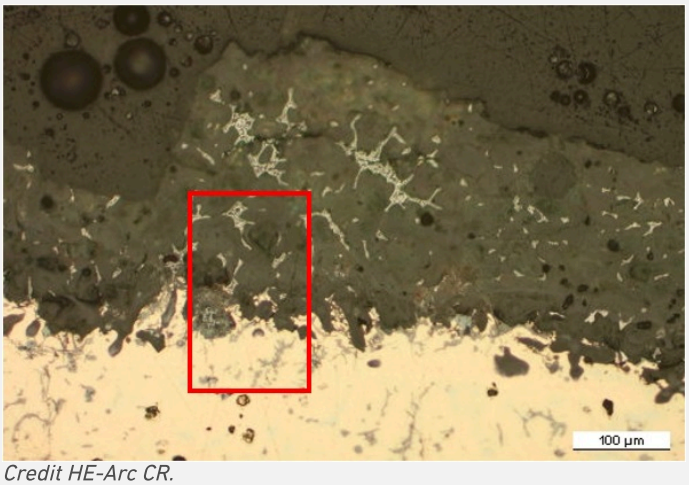

Credit HE-Arc CR.

Fig. 7: Micrograph of the metal sample from Fig. 3 (rotated 180°), unetched, bright field. A metallic ghost structure is preserved in the corrosion crust. The mapped area (Fig. 10) is marked by a rectangle,

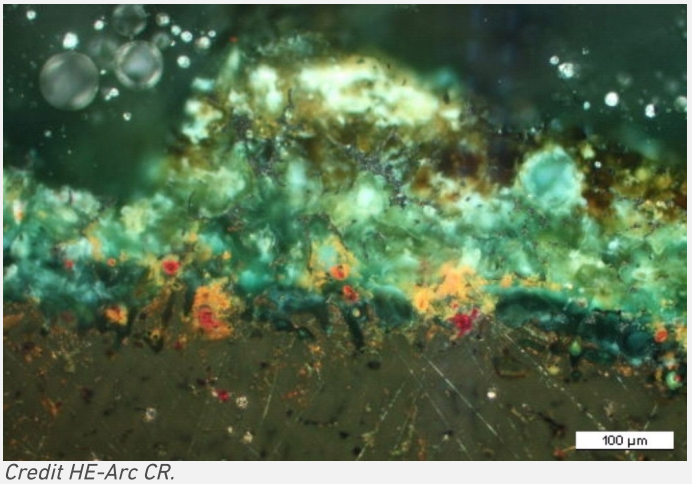

Credit HE-Arc CR.

Fig. 8: Micrograph similar to Fig. 7 and corresponding to the stratigraphy of Fig. 4, polarised light. At the metal - green corrosion crust interface red and orange corrosion products can be seen,

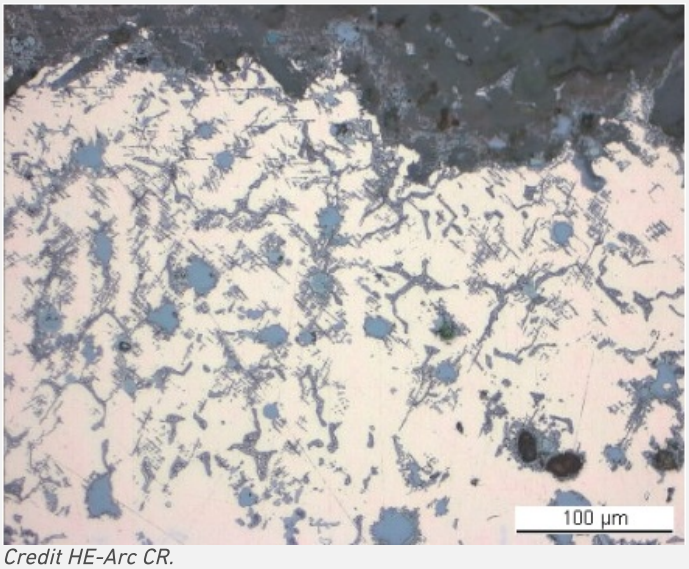

Credit HE-Arc CR.

Fig. 9: Micrograph of the metal sample from Fig. 3 (detail), unetched, bright field. Metal with slip lines outlined by the corrosion,

This work is licensed under CC BY-NC-ND 4.0

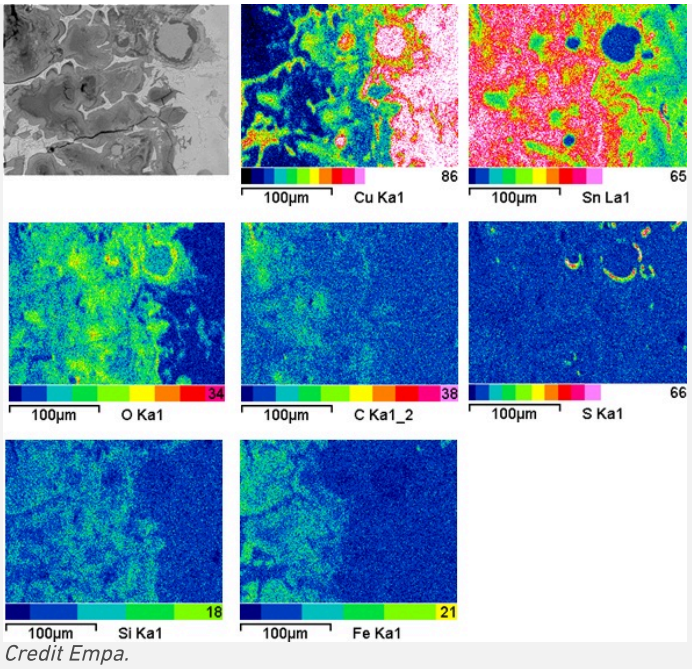

Credit Empa.

Fig. 10: SEM image, SE-mode, and elemental chemical distribution of the selected area of Fig. 7 (reversed picture rotated by 270°). Method of examination: SEM/EDS, Laboratory of Analytical Chemistry, Empa,

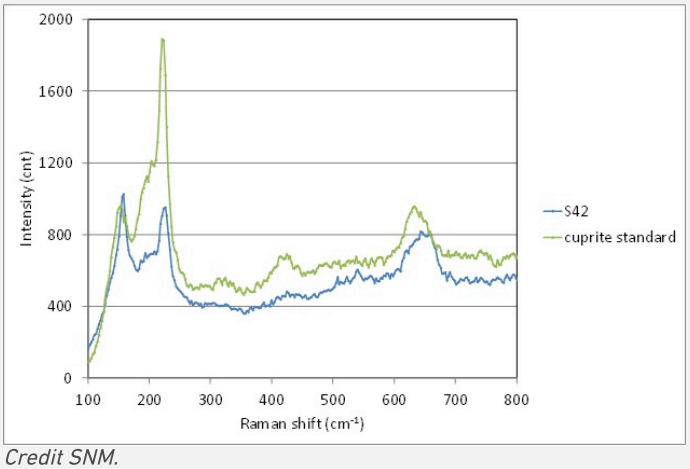

Credit SNM.

Fig. 11: Raman spectrum of a red-orange corrosion particle (S42) of Fig. 8 compared to the cuprite standard spectrum. Settings: laser wavelength 532nm, acquisition time 10s, one accumulation, filter D2 (0.75-0.8mW), hole 500, slit 80, grating 600. Method of analysis: Raman spectroscopy, Lab of Swiss National Museum, Affoltern a. Albis ZH,

Corrosion form	Uniform - selective
Corrosion type	Type I (Robbiola)

Complementary information

Nothing to report.

MiCorr stratigraphy(ies) – CS

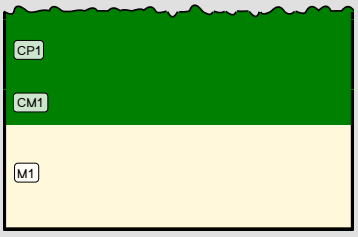

Fig. 4: Stratigraphic representation of the object in cross-section using the MiCorr application. This representation can be compared to Fig. 8.

Synthesis of the binocular / cross-section examination of the corrosion structure

This work is licensed under CC BY-NC-ND 4.0

Corrected stratigraphic representation: none.

Conclusion

The evenly corroded tin bronze contains numerous sulphide inclusions and shows signs of interdendritic corrosion penetrating the metal structure. The Sn enriched surface is decuprified and polluted by the environmental elements such as O, Si, Fe, C, Al and Cl. The corrosion crust is composed mainly of a dark green layer with local orange-red cuprite particles at the interface with the remaining metal. Both the remnant metallic phases and the Sn-rich corrosion layer can be interpreted as inferior markers, defining the limit of the original surface which is located above. For the above mentioned reasons, the corrosion is thought to be of type 1 according to Robbiola et al. 1998.

References

References on object and sample
Reference object
1. Fischer, C. (1997) Innovation und Tradition in der Mittel- und Spätbronzezeit. Monographien der Kantonsarchäologie Zürich 28, Zürich, 168.
Reference sample
2. Northover, P. (1997) Metalworking waste from Erlenbach-Obstgartenstrasse. In: Fischer, C. Innovation und Tradition in der Mittel- und Spätbronzezeit. Monographien der Kantonsarchäologie Zürich 28, Zürich, 99-101.
References on analytic methods and interpretation
3. Bertholon, R. (2001) Characterization and location of the original surface of corroded archaeological objects. Surface Engineering, 17 (3), 241-245. 4. Robbiola, L., Blengino, J-M., Fiaud, C. (1998) Morphology and mechanisms of formation of natural patinas on archaeological Cu-Sn alloys, Corrosion Science, 40, 12, 2083-2111.

This work is licensed under CC BY-NC-ND 4.0